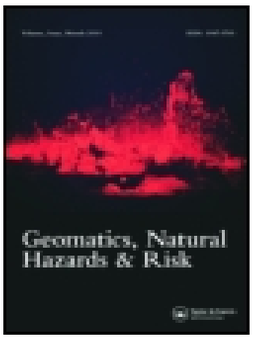

Geomatics, Natural Hazards and Risk

ISSN: 1947-5705 (Print) 1947-5713 (Online) Journal homepage: www.tandfonline.com/journals/tgnh20

Integrated geomatics for seamless coastal mapping: a vulnerable coastline in the central Adriatic Sea

Anna Nora Tassetti, Giorgio Simone, Gaspare Avanzato, Eva Savina Malinverni, Francesco Memmola, Maurizio Brocchini & Pierluigi Penna

To cite this article: Anna Nora Tassetti, Giorgio Simone, Gaspare Avanzato, Eva Savina Malinverni, Francesco Memmola, Maurizio Brocchini & Pierluigi Penna (2025) Integrated geomatics for seamless coastal mapping: a vulnerable coastline in the central Adriatic Sea, Geomatics, Natural Hazards and Risk, 16:1, 2584699, DOI: 10.1080/19475705.2025.2584699

To link to this article: https://doi.org/10.1080/19475705.2025.2584699

Published online: 18 Nov 2025.

GEOMATICS, NATURAL HAZARDS AND RISK
2025, VOL. 16, NO. 1, 2584699
https://doi.org/10.1080/19475705.2025.2584699

Taylor & Francis
Taylor & Francis Group

RESEARCH ARTICLE

OPEN ACCESS Check for updates

Integrated geomatics for seamless coastal mapping: a vulnerable coastline in the central Adriatic Sea

Anna Nora Tassetti[a], Giorgio Simone[b,c], Gaspare Avanzato[a,b], Eva Savina Malinverni[d], Francesco Memmola[e], Maurizio Brocchini[d] and Pierluigi Penna[a]

[a]CNR - IRBIM - National Research Council, Institute for Biological Resources and Marine Biotechnologies, Ancona, Italy; [b]Department of Biological, Geological and Environmental Sciences, University of Bologna, Bologna, Italy; [c]CNR - ISMAR - National Research Council, Institute of Marine Sciences, Bologna, Italy; [d]Department of Civil Engineering, Università Politecnica delle Marche, Ancona, Italy; [e]Dipartimento di Scienze della Vita e dell'Ambiente, Università Politecnica delle Marche, Ancona, Italy

ABSTRACT

The dynamic interface between land and sea - often referred to as the 'white ribbon' by the British Geological Survey - remains one of the most challenging zones for high-resolution surveying due to its inaccessibility to both traditional marine and terrestrial methods. Yet, this intertidal and nearshore region is critical for assessing coastal vulnerability, sediment dynamics, and erosion risk, especially under climate change pressures. This study presents an integrated geomatics-based approach to generate a seamless, high-resolution digital elevation model (DEM) for the vulnerable coastline of Sirolo (Central Adriatic Sea, Italy), characterized by steep cliffs and dynamic sedimentary processes. A suite of complementary datasets - including GNSS-derived elevation points, single- and multibeam echosounder data (via Autonomous Surface Vehicle and survey vessel), and UAV-based photogrammetry - were harmonized to bridge the coastal data gap. The resulting DEM supports numerical simulations to evaluate the effectiveness of adaptation measures and nature-based coastal defense strategies.

ARTICLE HISTORY
Received 24 May 2025
Accepted 19 October 2025

KEYWORDS
Digital elevation model; coastal hazard assessment; Integrated coastal mapping; sonar bathymetry; UAV photogrammetry

1. Introduction

Coastal systems represent some of the most valuable yet critically vulnerable environments globally (Fan et al. 2023; Dong et al. 2023). Climate change, sea level rise, and increasing storminess significantly alter coastal morphology and impact both coastal communities and ecosystems, heightening the demand for effective coastal erosion protection. This need is particularly urgent in areas where high vulnerability to climate change intersects with dense urban development and tourism-driven economies, as is the case in many Mediterranean coastal areas (Baldoni et al. 2024). In such contexts, there is an urgent demand for timely, accurate, and spatially detailed geospatial data to inform evidence-based coastal management, risk reduction, and climate adaptation strategies (Ahmed et al. 2025).

A fundamental component of effective coastal management is the regular and precise mapping of shoreline position and elevation - encompassing both topographic and bathymetric data - especially in the nearshore zone where land and marine processes interact (Uunk et al. 2010; Bonaldo et al. 2019; Laignel et al. 2023; Dike et al. 2024). Yet, collecting high-resolution geospatial data in shallow coastal waters continues to pose significant technological and operational constraints (Salameh et al. 2019; Xu et al. 2025). This transitional zone - often referred to as the 'white ribbon', a term introduced by the British Geological Survey - remains a persistent critical data gap, due to its complex hydrography and limited accessibility by both traditional marine and land-based surveying techniques (Carvalho et al. 2017; Alevizos et al. 2022). Addressing this challenge is essential to advancing integrated, multi-scale assessments of coastal vulnerability and to supporting sustainable planning in hazard-prone coastal regions.

CONTACT Anna Nora Tassetti annanora.tassetti@cnr.it

Article highlights

- A seamless Digital Elevation Model (DEM) was created by combining UAV photogrammetry, single-beam and multibeam sonar, and RTK-GNSS surveys, to map a complex coastline.
- The study addressed a critical data void in the shallow nearshore zone—often inaccessible to both terrestrial and marine survey methods—using an innovative multi-platform approach.
- The resulting DEM enabled advanced numerical simulations to assess coastal vulnerability and the effectiveness of nature-based defense measures.
- The integration of low-cost UAV and ASV systems demonstrated a scalable and practical method for topobathymetric mapping in morphodynamically active coastal settings.

State-of-the-art technologies such as echo sounders and airborne LiDAR bathymetry offer high accuracy and reliability. Airborne LiDAR bathymetry is capable of rapidly surveying nearshore areas down to approximately 20 meters depth, depending on water turbidity and surface wave conditions, and operates without many of the constraints faced by marine-based systems. However, its high costs, technical complexity, and limited scalability for frequent, large-area surveys constrain its widespread use (Mudiyanselage et al. 2022). Conventional hydro-acoustic methods, such as boat-mounted MultiBeam EchoSounders (MBES), remain the standard in studies requiring high-resolution and full-coverage depth measurements. These systems provide valuable insights into underwater morphology and are extensively used in coastal research (Hughes Clarke et al. 1996; Tassetti et al. 2015; Holland et al. 2021; Somoza et al. 2021). Nonetheless, their effectiveness diminishes in shallow, hazard-prone waters, where obstacles like rocks, reefs, and swimmers pose safety risks and limit vessel maneuverability (Kenny et al. 2003; Agrafiotis et al. 2019; Shih et al. 2024). Simultaneously, this transitional nearshore zone is often too deep for land-based survey techniques and too turbid for passive optical satellite-derived bathymetry to function reliably (Li et al. 2022; Saeidi et al. 2023). Onshore, traditional topographic methods like RTK-GNSS and total stations deliver high-precision topographic data but are frequently impractical for covering large or inaccessible areas such as cliffs and rugged terrain (Mills et al. 2005; Cooper et al. 2021). While airborne photogrammetry and LiDAR scanning can overcome these challenges by offering broader coverage, their high cost often makes them unsuitable for localized or regularly repeated surveys (Pirasteh and Li 2017). In contrast, small Unmanned Aerial Vehicles (UAVs) have emerged as a cost-effective and practical alternative for high-resolution topographic data, especially over small to medium extents (Buffi et al. 2017; Alevizos et al. 2022).

As a result, comprehensive, high-resolution datasets that seamlessly span the coastal interface - from the subtidal zone through the intertidal and up to the supra-tidal backshore - remain rare and challenging to acquire (Leon et al. 2013). This persistent 'white ribbon' gap limits the ability to model coastal processes accurately or to assess and design nature-based or engineered adaptation solutions (Ward et al. 2020).

In response to these challenges, numerous studies have explored methods to create seamless digital elevation models (DEMs) across the land-sea interface. These include integrating data from diverse data sources, including GPS, LiDAR, single- and multibeam echosoundings, satellite imagery, and nautical charts (Westhead et al. 2014; Danielson et al. 2016; Lubczonek et al. 2021; Włodarczyk-Sielicka et al. 2022; Lewicka et al. 2022). Quadros et al. (2008) investigated the integration of independently acquired topographic and bathymetric LiDAR datasets to produce a continuous DEM of Port Phillip Bay. Danielson et al. (2016) presented an enhanced methodology for generating coastal topobathymetric DEMs by merging topographic datasets with adjacent intertidal and offshore bathymetric data. In a UAV-based application, Starek and Giessel (2017) proposed a data acquisition and processing workflow using a Sensefly eBee equipped with a Canon IXUS 127 HS digital camera to generate a hybrid topo-bathy DEM. Similarly, Legleiter (2012) demonstrated a hybrid technique for mapping riverine morphology by combining LiDAR-derived topography with spectral-based bathymetry. Earlier efforts by Gesch and Wilson (2001) resulted in the development of a seamless topographic/bathymetric elevation model for Tampa Bay, integrating disparate datasets from the USGS National Elevation Dataset and NOAA digital soundings. Freeman et al. (2004) also addressed the complexities of high-resolution coastal DEM production, proposing a workflow based on real-time kinematic GPS and ultra-shallow water sonar to overcome challenges related to oversampled datasets and data processing.

In this context, this study proposes a multi-sensor, integrated approach to map a highly vulnerable coastal area along the central Adriatic Sea. Characterized by steep cliffs, narrow beaches, and active sediment dynamics, the site serves as a representative case for testing advanced coastal monitoring methods. Topobathymetric data were collected using four complementary techniques: (i) a hull-mounted MBES for deeper subtidal zones, (ii) an Autonomous Surface Vehicle (ASV)-based Single-Beam EchoSounder (SBES) for shallow water mapping, (iii) RTK-GNSS for high-precision topographic data in accessible areas, and (iv) UAV photogrammetry for high-resolution 3D surface reconstruction of the above-water terrain.

The primary objective was to generate a seamless, high-resolution DEM that supports numerical modeling of coastal morphodynamics and facilitates the evaluation of site-specific adaptive measures aimed at enhancing coastal resilience. This work is part of a broader interdisciplinary project aimed at characterizing the geological-geomorphological, oceanographic, and ecological settings of the Sirolo coast to inform the development of sustainable, science-based resilience strategies.

1.1. Study area

The case study is located along the southwest coast of the Conero Promontory within the municipality of Sirolo on Italy's central Adriatic coast. The area extends about 2 nm alongshore and 1 nm offshore, from the northern beach of the municipality of Numana to the iconic 'Due Sorelle' beach (Figure 1). The stretch is dominated by Monte Conero cliff (*N* 43 ° 33.06' E 13 ° 36.3'), a prominent cliff rising to 572 meters above sea level - the highest relief along the Adriatic coastline.

The geomorphological condition of the area is shaped by geological processes and active marine erosion, resulting in a rugged landscape of white-pebbled coves, narrow beaches, and small gulfs. Beaches mainly consist of pebbles and angular breccias, with sand appearing only occasionally. The nearshore seabed is largely rocky with scattered sand patches, gradually giving way to mobile sediments and low-relief outcrops further offshore.

Coastal morphogenesis is driven by both gravitational and marine processes, creating diverse slope landforms and sedimentary deposits. Landslides of varying types and activity levels are widespread along the coastal slope and contribute to shoreline evolution and sediment supply (Troiani et al. 2020). The dominant wind regime, from the SSE–SSW sectors, generates southeast-directed waves. During winter storms, wave heights can reach 3 to 3.5 meters, especially under Bora wind conditions, when waves from the northeast (NE) strike the coastline as a secondary direction. The average tidal range is modest (approx. 0.5 meters), and tidal currents play a minor role in sediment transport.

Ecologically, the area is highly significant. It lies within the Conero Nature Park, established in 1987 to protect 6,011 hectares across Ancona, Camerano, Numana, and Sirolo. The site is part of the Natura 2000 network, designated as a Site of Community Importance (SCI IT5320006, titled 'Portonovo and limestone cliffs by the sea') and a Special Protection Area (SPA IT5230007) under EU conservation directives. Protected habitats include shallow bays, submerged reefs, and intermittently exposed sandbanks, supporting rich marine biodiversity. These characteristics make the area both a conservation priority and a natural laboratory for studying interactions between geomorphic processes and coastal ecosystems in a Mediterranean context.

2. Materials and methods

The coastal zone was divided into three elevation domains based on geomorphology and survey feasibility: (i) supratidal, (ii) transitional (spanning from the intertidal area up to approximately 4 meters in depth), and (ii) offshore (beyond the 4-meter isobath). UAV photogrammetry, ASV-based SBES, and hull-mounted MBES were respectively employed to map each domain. This integrated survey design enabled the creation of a seamless high-resolution DEM across the land–sea interface, ensuring both data continuity and vertical consistency.

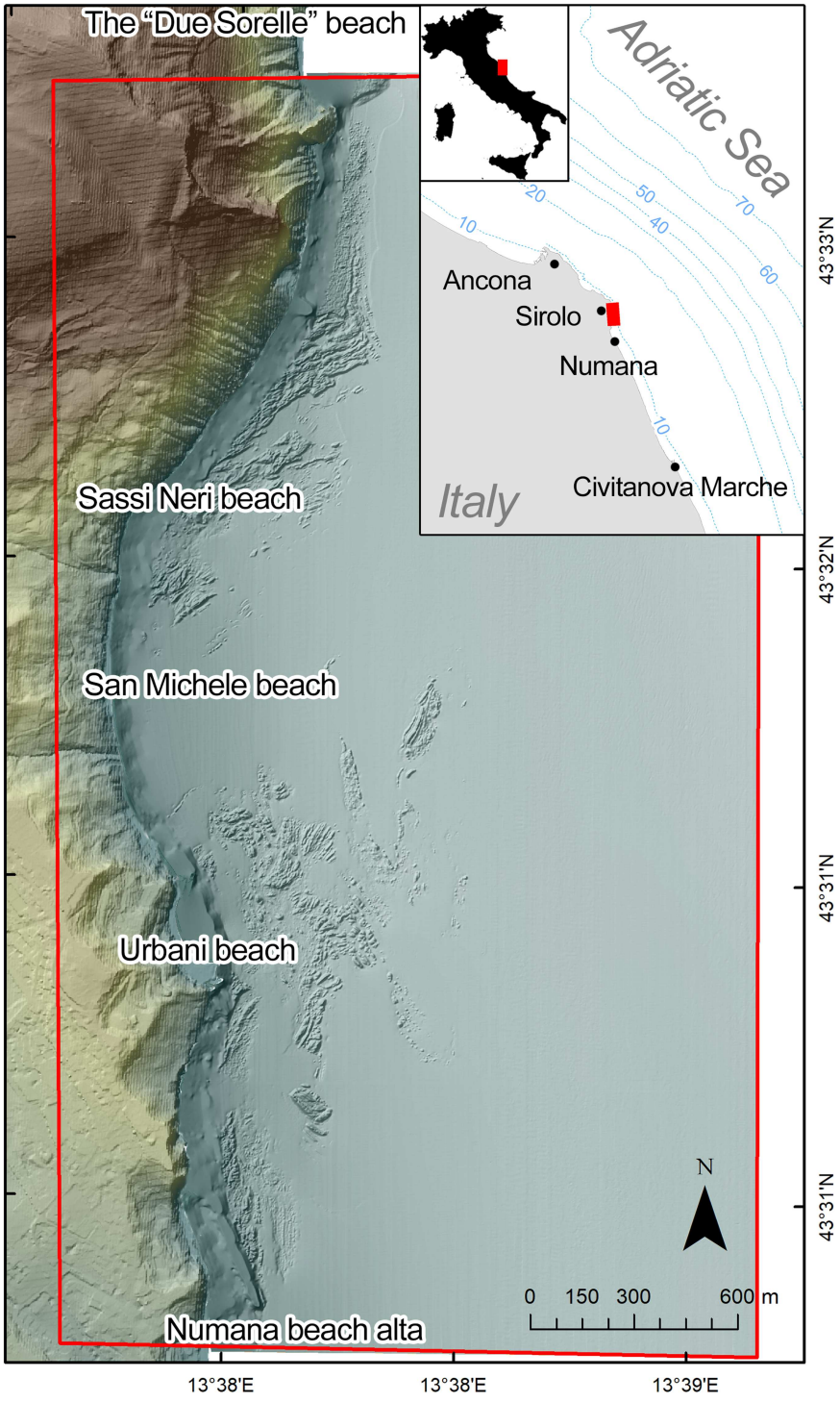

Figure 1. Case study area (outlined in red), LiDAR-derived DTM (source: wms.pcn.minambiente.it) and the acquired SBES/MBES bathymetry.

2.1. Direct survey of the coastline

In July 2023, accessible portions of the coastline were surveyed using a dual-antenna RTK-GNSS system. Surveys were conducted along cross-shore profiles extending to approximately 1 meter in depth, specifically targeting the transition zone between the terrestrial UAV-derived point cloud and the shallow-water SBES sonar data. The RTK-GNSS points served to validate the topographic surface derived from UAV

photogrammetry, as well as validate/co-register the adjacent SBES bathymetric data, ensuring vertical consistency across the land–sea interface.

Due to budgetary limitations, UAV coverage did not extend across the full study area. To ensure continuity in the coastline delineation, the Regional Technical Map (CTR 1:10,000) provided by the Marche Region (https://www.regione.marche.it) was used to extrapolate shoreline features beyond the UAV survey extent.

2.2. UAV photogrammetry

Elevation data for the first domain - covering the supratidal and terrestrial portions of the coastal zone - were acquired using a DJI Phantom 4 Pro UAV equipped with a 1-inch, 20-megapixel CMOS sensor, supported by a Geomax Zenith 35-PR GNSS receiver for precise geolocation (Figure 2, right). The photogrammetric survey was conducted in October 2023, following the official authorization from Conero Nature Park Authority (*Environmental Impact Screening Advice, Directorate Determination No. 35, dated 01/10/2023)*. Due to the steep and rugged terrain of the Conero coastline, flights were manually piloted by an operator, capturing both oblique and nadiral (camera angle at 90° to the horizon) imagery at an altitude of less than 100 meters above ground level. To ensure high geospatial accuracy, a network of 30 Ground Control Points (GCPs) was established along the shoreline. These GCPs were measured using the aforementioned RTK-GNSS system, achieving a positional accuracy of ±5 cm and referenced to the Monte Mario/Italy Zone 2 coordinate system.

Post-processing was performed using Agisoft Metashape Professional 1.7.4, applying Structure-from-Motion (SfM) photogrammetry techniques and including the following key steps: (i) Image alignment: detection of tie points and generation of a sparse point cloud; (ii) Georeferencing: Integration of GCPs to optimize spatial accuracy; (iii) Bundle adjustment and camera calibration: refinement of internal camera parameters and point alignment; (iv) Dense point cloud generation: creation of a high-resolution 3D model with RGB texture; (iv) Orthomosaic generation: production of georeferenced nadiral imagery; (v) DEM extraction: interpolation of elevation points onto a regular grid. The final dense point cloud was gridded at a 6 cm spatial resolution, while the orthomosaic was produced at 3 cm resolution, yielding high-accuracy topographic datasets well-suited for seamless integration with sonar-derived bathymetric data in the coastal transition zone.

Figure 2. The OpenSWAP ASV equipped with SBS during the shallow-water bathymetric survey (left), and the DJI Phantom 4 Pro UAV during the aerial photogrammetry campaign (right).

2.3. Single-beam bathymetry

To map the second elevation domain, spanning the transition zone from the intertidal area to nearshore waters at depths of approximately 2.5 to 3.0 meters, bathymetric data were acquired using the OpenSWAP ASV (Figure 2, left). Developed as an open-source platform for shallow-water geophysical monitoring (Stanghellini et al. 2020; Stanghellini et al. 2022), OpenSWAP is a lightweight, modular, and portable plastic catamaran powered by electric propulsion.

The survey was conducted in September 2023, with the OpenSWAP equipped with: (i) an RTK GPS, (ii) an autonomous navigation system integrated with inertial sensors and (iii) a precision SBES capable of seabed detection and SEG-Y data output. The sonar system consisted of a 200 kHz vertical-incidence ultrasonic pinger, featuring an 8 ° conical beam width and a 350 μsec pulse length, optimized for shallow-water operation and reduced bottom detection ambiguity. Survey lines were oriented perpendicularly to the shoreline and underwater slope, with slight overlap into the adjacent MBES coverage area to ensure spatial continuity and facilitate data integration. Line spacing was set between 60 and 80 meters, being forced to balance spatial resolution requirements with operational and budget constraints. The SwapCONTROLLER software was used to predefine navigation paths and to manually operate the ASV near obstacles or rocky outcrops using joystick control, thereby enhancing safety in complex nearshore environments. Under suitable environmental conditions, the OpenSWAP maintained high positional accuracy along the pre-programmed navigation paths, and reliable seabed detection.

Post-processing of raw echo soundings was carried out using the BeamworX software suite (BeamworX BV, Utrecht, the Netherlands), with necessary corrections applied for transducer draft and tidal fluctuations. Tidal corrections were based on water level data from the Ancona tide-gauge station (~20 km north of the study area), part of the Italian national tide gauge network (www.mareografico.it). These data were time-synchronized via the GNSS receiver, and the vertical reference was adjusted to Mean Sea Level (MSL) accordingly.

2.4. Multibeam bathymetry

Elevation data for the third domain, extending from the nearshore limit to offshore waters were collected using a Kongsberg EM2040CD MBES installed aboard the 14-m-long RV Tecnopesca II. The survey was conducted over eight days in July–August 2023, with operations limited to periods outside official bathing hours (08:00–18:00), in accordance with Ordinance No. 59 issued on 10/07/2023 by the Ancona Harbor Master's Office. Due to navigational safety constraints in shallow waters, the MBES survey began at depths between 3.5 and 4 meters, complementing the shallower SBES coverage. The EM2040CD, a compact dual-transducer version of the EM2040, is optimized for seafloor-echo detection at ranges below 600 m. Each transducer, hull-mounted at ~0.8 m depth below the waterline, yields a 2D fan of 400 beams, enabling dense sampling of both bathymetry and backscatter intensity. Real-time sound speed correction was applied using a Valeport miniSVS sensor positioned near the transducers. In addition, Sound Velocity Profiles (SVPs) were acquired twice daily using an AML Smart SV&P profiler, as water column stratification remained minimal throughout the survey due to stable meteorological and oceanographic conditions. Vessel motion was corrected in real time using a Kongsberg Seatex MRU 5 motion sensor and an Anschütz Gyro Compass Standard 20 Compact Type 110–222 NG001. Positioning was provided by a Trimble SPS855 GNSS Modular Receiver, with all systems synchronized to UTC via GPS. Each acoustic ping recorded beam steering angle, sample range, backscatter magnitude, and navigation/attitude data into ALL binary files, ensuring full integration of positional and acoustic information.

A total of 207 survey lines were acquired, arranged as evenly spaced, parallel transects in alternating north–south directions. Survey speed ranged from 4 to 5 knots, with a central operating frequency of 360 kHz. Line spacing was dynamically adjusted based on water depth to ensure at least 20% swath overlap. In areas with complex bathymetry, transects were modified in real time to enhance coverage and account for topographic irregularities. Overlapping swaths provided redundancy, mitigating data gaps from sudden topographic changes or sharp vessel maneuvers.

Post-processing was performed using QPS Qimera 2.5.4 (Quality Positioning Services BV, Zeist, the Netherlands), and it was focused on removing navigational errors, beam anomalies and noise, as well as applying sound velocity corrections. Tidal corrections were derived from the Ancona tide-gauge station, part of the Italian national tide gauge network (www.mareografico.it), and referenced to MSL.

2.5. Data integration

Following consistency and quality assurance checks - particularly regarding vertical datum alignment - all elevation datasets were integrated into a unified surface model. The process involved harmonizing the UAV-derived topographic data, SBES and MBES bathymetry, and RTK-GPS shoreline control points, ensuring continuity across the land–sea interface.

Prior to integration, all datasets were converted to XYZ point format and projected into a common reference system. Elevation points within 200 meters of the shoreline, including terrestrial and sonar data, were interpolated using the *Topo to Raster* tool in ArcGIS, which implements the ANUDEM thin plate spline algorithm (Hutchinson 2000; Hutchinson et al. 2011). This method is particularly effective for generating continuous elevation surfaces from heterogeneous point clouds. To reduce edge effects, the final topographic grid was clipped to include land elevations within 100 meters of the shoreline—half the original buffer zone. In the final processing step, the interpolated bathymetry grid (used in Figure 1) and the UAV-derived topographic grid were mosaicked. Within the 100-meter overlap zone, a weighted averaging GIS function was applied to blend cell values based on their proximity to the grid edges, ensuring a smooth transition between datasets.

While UAV-derived SfM points were initially included, those intersecting the shallow-water domain covered by sonar data were excluded from the interpolation. This was necessary because photogrammetric models tend to misrepresent water surfaces, where reflectivity and transparency often lead to distortion (Szostak et al. 2024). To ensure dataset separation, the same coastline vector was used to mask terrestrial areas prior to rasterizing the sonar-derived point clouds, ensuring that only underwater points were used in the bathymetric interpolation. A final 1-meter grid spacing was selected for interpolation, balancing the need for spatial detail with the resolution constraints of the input datasets.

2.6. Accuracy assessment

To ensure seamless DEM integration, vertical and horizontal accuracy of each dataset was quantified using the Root Mean Square Error (RMSE):

$$\mathrm{RMSE} = \sqrt{\frac{\sum (X_{measured} - X_{reference})^2}{n}}$$

where $X_{measured}$ is the elevation or planimetric coordinate from the dataset under evaluation, and $X_{reference}$ is the corresponding value from an independent, higher-accuracy reference.

- *RTK-GNSS*: Precision was assessed from repeated benchmark measurements and validated against the Italian national GNSS reference network.
- *UAV Photogrammetry*: Vertical ($RMSE_z$) and horizontal ($RMSE_{xy}$) accuracies were computed using 20 independent RTK-GNSS checkpoints not used as GCPs.
- *SBES Bathymetry*: $RMSE_z$ was calculated from point-by-point comparisons with MBES data in the overlap zone and with nearshore GNSS survey points.
- *MBES Bathymetry*: $RMSE_z$ was estimated from overlap with SBES points and theoretical uncertainties from positioning, motion, and sound velocity sensors. Data quality was verified against IHO S–44 standards.
- *Cross-Dataset Consistency*: All overlap zones were tested, adopting an acceptance threshold of ±0.10 m $RMSE_z$.

3. Results

A total of 380 RTK-GPS points, including 350 collected along cross-shore profiles and 30 evenly distributed across the flight area, were collected with centimeter-level accuracy, serving both as ground control data for the topographic surface derived from UAV imagery and as tie points for integrating and aligning AUV and SBES elevation datasets (Figure 3A and Figure 4C). These reference points played a key role in geo-locating the SBES sonar profiles and minimizing spatial discrepancies during data fusion.

The UAV photogrammetric survey covered an area of approximately 57 hectares and used 770 aerial images. These were captured in timed shooting mode, with an 80% overlap in both the horizontal and vertical directions to ensure sufficient coverage and image correlation. Accuracy requirements were ensured using the 30 GCPs acquired with an estimated GNSS positional accuracy of ±5 cm. A multiple bundle adjustment was applied to the sparse point cloud to refine camera calibration and spatial alignment. The final orthomosaic and digital surface model (DSM, that follows vegetation) achieved average ground resolutions of 3.07 cm/px and 6.14 cm/px, respectively (Figure 3). The overall $RMSE_z$ calculated from the GCPs was 3.6 cm, indicating high positional accuracy across the dataset.

Approximately 325,000 SBES points were acquired within the shallow-water zone, overlapping MBES soundings (Figure 4A). Overlapping zones between SBES and MBES soundings (Figure 4C) were critical for quality assurance and were closely examined for vertical consistency. Discrepancies were within ±10 cm, largely attributed to differences in beam geometry and operating frequency between the two sonar

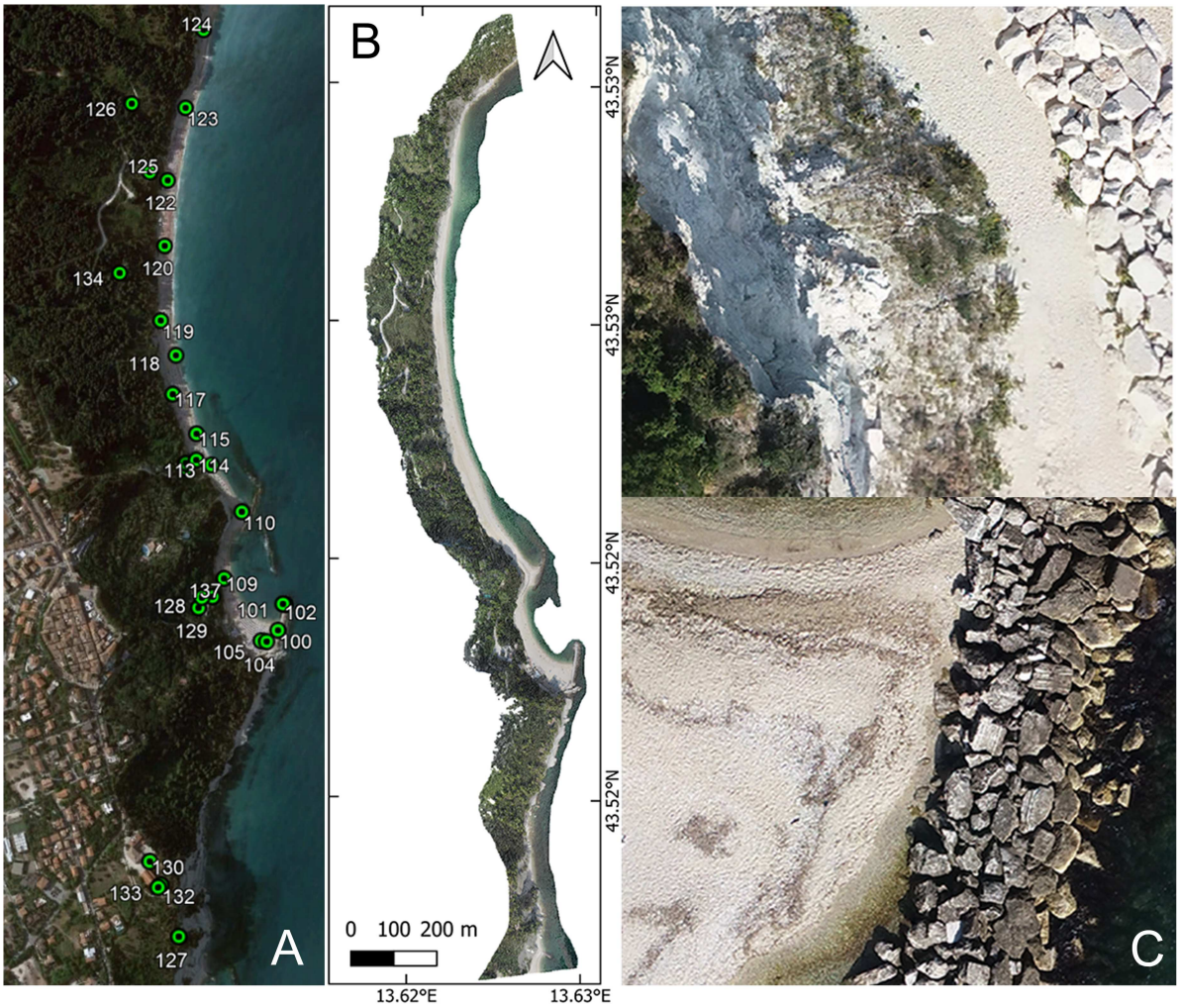

Figure 3. Positions of the GCPs (green points, A), DSM overlain by the orthomosaic (B), detail views of the orthophoto (C).

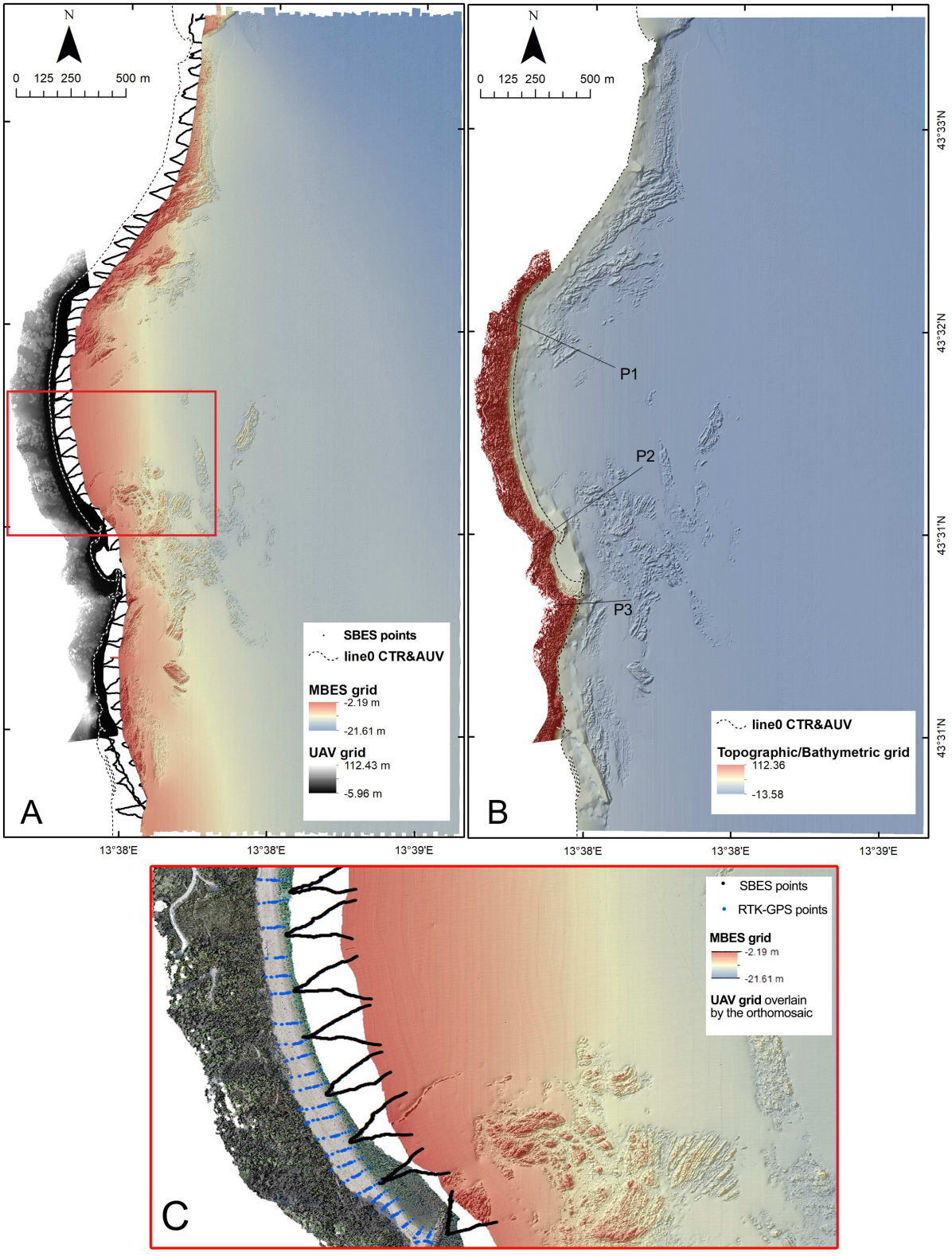

Figure 4. Multiple elevation data sources (A) and detail view (C): MBES grid (depth >3.5/4m), SBES points (depth <3.5/4m), and above-water SfM textured grid; Data integration and final topographic/bathymetric elevation model (EPSG: 32633, 1 m resolution, B).

systems. Although the SBES system does not provide full swath coverage, the OpenSWAP platform's high positional accuracy and suitability for shallow-water operations enabled reliable acquisition of point-sounding data in a previously unmapped sector. However, the absence of dense cross-track coverage necessitated the use of extensive spatial interpolation techniques to generate a continuous bathymetric surface and bridge gaps between SBES survey lines. This interpolation step was essential to enable integration with adjacent UAV and MBES datasets for seamless DEM generation.

The MBES bathymetric dataset covered an area of approximately 5.7 km², encompassing water depths ranging from 2.8 m to ~14 m (Figure 4A). The processed bathymetric surface was referenced to MSL, projected to UTM Zone 33 N (WGS84) and exported in XYZ ASCII and GeoTIFF formats at a 0.5-meter grid resolution, providing a detailed and accurate representation of offshore seabed morphology. Although the survey was not intended for navigational safety purposes, bathymetric data uncertainty was assessed using Qimera v.2.5.4 and following the IHO Standards for Hydrographic Surveys (S–44, 6th Edition, 2022). Total Horizontal Uncertainty (THU) and Total Vertical Uncertainty (TVU) were computed by accounting for the standard deviation offsets of the motion reference unit (MRU), MBES, sound velocity sensors, and GNSS-based positioning system. Input parameters were derived from the MBES technical datasheets and the installation configuration report. Notably, uncertainty values for the Kongsberg EM2040 system varied depending on both sampling frequency and depth fluctuations encountered during the survey. Therefore, the reported uncertainty ranges correspond to values calculated for the 360 kHz operating frequencies and the range of pulse lengths employed during data acquisition. The resulting horizontal and vertical uncertainties complied with IHO Exclusive Order specifications and met the more stringent standards of LINZ (THU: 1.25 m; TVU: 0.29), confirming that the quality was sufficient to support high-resolution bathymetric mapping and satisfied the accuracy requirements of the survey's scientific objectives.

The data acquisition techniques and corresponding datasets are summarized in Table 1, while their respective spatial extents are shown in Figure 4A.

The accuracy assessment quantified vertical and horizontal errors for each dataset, as well as consistency across overlap zones; the results are summarized in Table 2.

Spanning approximately 2 nautical miles alongshore and 1 nautical mile offshore, the final merged elevation model maintained spatial coherence and minimized vertical discontinuities across sensor boundaries (Figure 4B). The resulting surface offers a realistic and clear portrayal of the coastal terrain in the case study, as evidenced by the cross-shore profiles in Figure 5 and the 3D visualization in Figure 6. A 1-meter spatial resolution was selected to support hydrodynamic and morphodynamic numerical

Table 1. Specific elevation datasets employed.

Elevation source	Elevation range	Typology	Spatial resolution
AUV photogrammetry	>0 m	grid	6 cm
GPS RTK	0 m	points	-
ASV SBES	[0, –4] m	points	-
MBES	<–4 m	grid	0.5 m

Table 2. Accuracy assessment summary for each dataset. Vertical ($RMSE_z$) and horizontal ($RMSE_{xy}$) errors are reported, along with cross-validation in overlap zones between datasets. All values satisfied the acceptance threshold for seamless DEM integration.

Elevation source	Reference source	$RMSE_z$ (m)	$RMSE_{xy}$ (m)	Notes
AUV Photogrammetry	20 GNSS Independent Check Points	0.04	0.03	Dense GCP network, SfM processing Environmental conditions main error sources Distortions over reflective water surfaces
GPS RTK	Repeat benchmark measurements + GNSS ref network	0.01	0.01	High positional repeatability
ASV SBES	MBES overlap zone + GNSS nearshore points	0.08	-	Beam width and shallow-water dynamics main error sources Reduced point density
MBES	SBES overlap zone	0.06	-	IHO S–44 Exclusive Order
Cross-Dataset (All)	Overlapping zones	0.09		Below ±0.10 m vertical tolerance

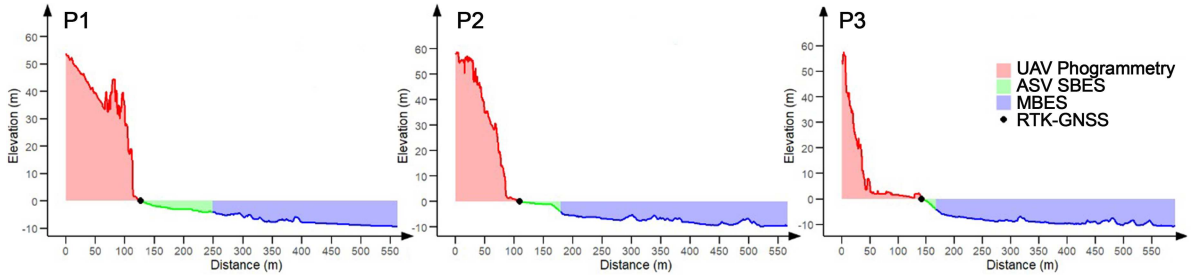

Figure 5. Cross-shore profiles covering all the combined data. Their locations are indicated in Fig 4B.

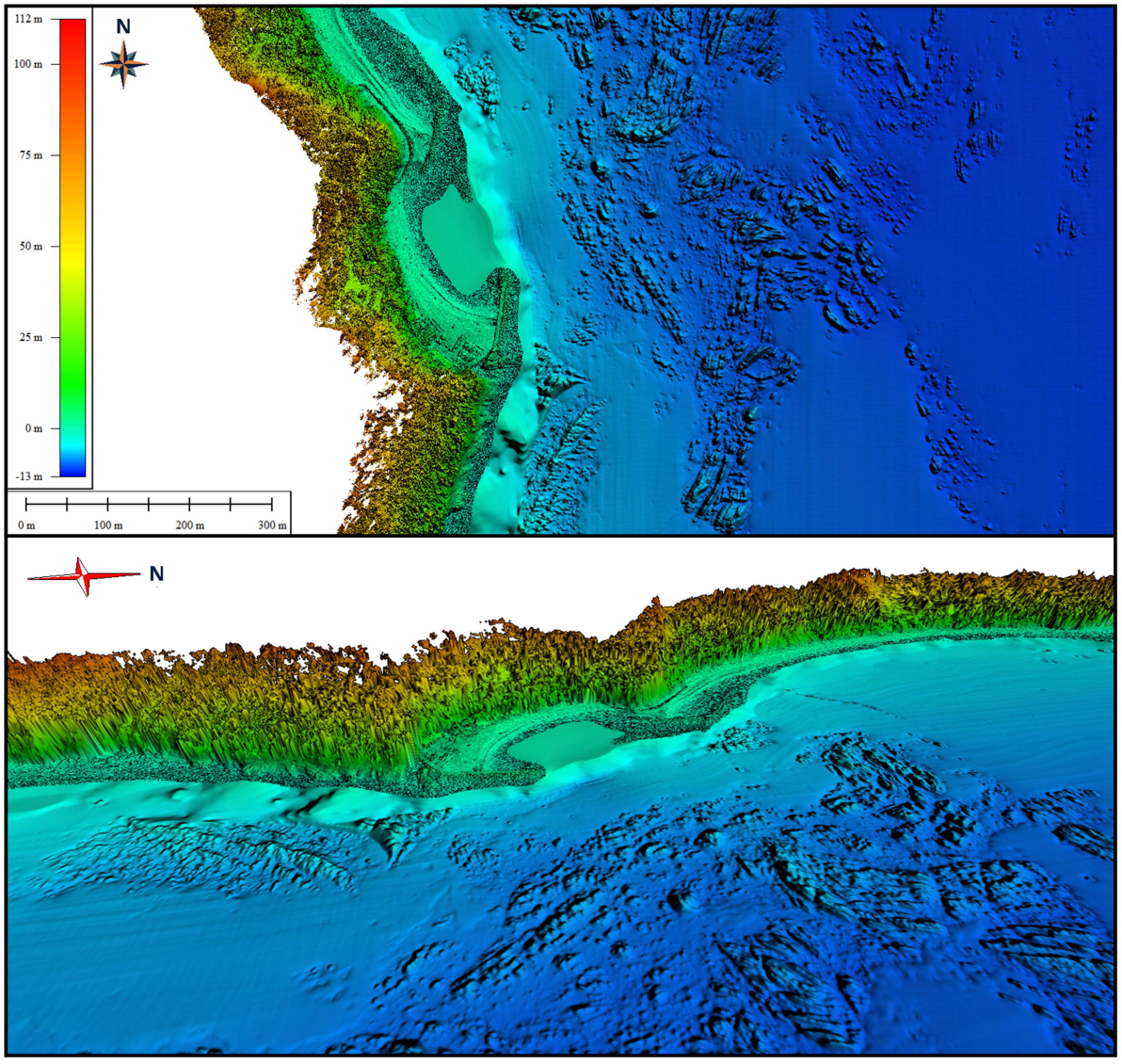

Figure 6. 3D visualization of the final seamless DEM.

modeling, providing an optimal balance between the native resolutions of the input datasets, ranging from 3–6 cm for UAV-derived topography, 50 cm for MBES, to coarser interpolated SBES data.

4. Discussion and conclusions

Although MBES systems have advanced considerably in recent decades - offering high-resolution, wide-swath bathymetric data capable of capturing detailed seafloor morphology (Madricardo et al. 2019; Foglini

et al. 2025) and increasingly for water-column imaging (Colbo et al. 2014; Minelli et al. 2021) - their use in very shallow-waters remains limited. Operational constraints, including the need for sufficient vessel draft, safety margins near complex coastlines, and the high cost and time requirements associated with achieving full coverage, often render MBES surveys impractical or economically unfeasible for nearshore applications. This is particularly true in studies with limited budgets or access restrictions, as was the case in the present survey.

In contrast, the SBES system, despite its lower spatial coverage, offered a cost-effective and operationally feasible alternative in shallow-water, especially where full insonification with MBES would be time-prohibitive or - as in the case study - beyond project constraints/client's budget. In such shallow-water, UAV photogrammetry was also proved unreliable due to surface water distortion effects.

Survey performance was influenced by environmental conditions such as wind and waves for UAV imagery and surface chop or turbidity for SBES. To mitigate these effects, data collection was limited to calm sea states, with UAV flights manually piloted at low altitude for stable image capture. These precautions minimized, though did not entirely eliminate, potential environmental biases.

A core challenge in constructing a seamless DEM from multi-source elevation data lies in reconciling disparate datasets (Leon et al. 2013), each with its own resolution, accuracy, acquisition geometry, and data format. Dataset accuracy was verified before integration by computing RMSE values for each dataset (Table 2).

In this study, the adoption of a smooth, hydrologically correct interpolation method - specifically, the *Topo to Raste*r tool - proved effective, provided the chosen grid resolution exceeded the coarsest input resolution. Designed to support the integration of irregular and unevenly spaced elevation inputs, the employed smooth interpolator is based on a discretized thin-plate spline formulation (Wahba 1990), adapted with a roughness penalty function that preserves sharp terrain features such as ridges, cliffs, and escarpments, which are prevalent in the Conero Promontory setting.

Interpolation gaps in the shallow transition zone were minimized by leveraging overlapping datasets. The merging process indeed involved surface interpolation across the overlapping areas, incorporating points from all the data sources, followed by raster mosaicing with weighted average data blending to minimize discontinuities at data boundaries. Although the bathymetric data could have been gridded independently, incorporating shoreline elevation points into the interpolation improved the continuity and realism of the land–sea transition. The interpolation was both visually and statistically assessed for artificial artifacts or inconsistencies, particularly at the land–sea boundary. Importantly, the *Topo to Raster* approach retained the original elevation ranges and generated a visually coherent and topographically realistic surface that is suitable for geovisualization, geomorphometric analysis, and subsequent numerical modeling. A 1-meter spatial resolution was adopted as a practical compromise between the varying native resolutions of the input datasets and the scale demands of subsequent numerical models simulating wave propagation and coastal interactions.

Results demonstrate the feasibility of creating a seamless, high-resolution DEM across the three defined elevation domains by integrating low-cost UAV photogrammetry, ASV-based SBES, RTK-GNSS and vessel-based MBES data, while ensuring continuous spatial coverage and vertical consistency. However, due to the heterogeneous nature of the source data - in both density and accuracy - users should be aware of spatial variability in the final model quality. While data resolution offshore and on land often supported high-resolution gridding, nearshore areas relied on interpolation across wider gaps, potentially reducing local accuracy. Vertical accuracy also fluctuates across the DEM, influenced by differences in acquisition dates, technologies, and sensor-specific characteristics. However, the systematic accuracy assessment (±0.10 m RMSE threshold across overlap zones, Table 2) confirmed that such discrepancies remained within acceptable limits, preserving the reliability of the final DEM for coastal hazard modeling and enhancing the replicability of the workflow in other coastal contexts. This is particularly important given that, alongside hydro-meteorological inputs, elevation data were a fundamental requirement for the subsequent coastal hazard modeling. The vertical accuracy of these datasets is critical, as even minor errors can significantly affect simulated inundation depths and extents, especially in low-gradient or nearshore flood-prone areas (Meadows et al. 2024).

In particular, a model-chain approach was adopted, integrating multiple numerical models to simulate coastal processes at various spatial and temporal scales (Memmola et al., unpublished data). Offshore wave

and circulation conditions were simulated using the wave driver Simulating WAves Nearshore (SWAN, Booij et al. 1999) and the circulation model Regional Ocean Modeling System (ROMS, Haidvogel et al. 2008) coupled within the Coupled Ocean-Atmosphere-Wave-Sediment Transport modeling framework (COAWST, Warner et al. 2010). This coupled modeling approach provided consistent boundary conditions for detailed nearshore hydro-morphodynamic simulations. ROMS is a three-dimensional, free-surface, terrain-following model that solves the Reynolds-averaged Navier-Stokes equations, while SWAN is a third-generation spectral wave model that solves the spectral action balance equation to simulate wave propagation and transformation. For nearshore hydro-morphodynamic analysis, ROMS was one-way coupled with the non-hydrostatic version of the XBeach circulation model (Smit et al. 2010), a two-dimensional, vertically-averaged model that solves the nonlinear shallow water equations (NSWE) in its non-hydrostatic configuration. XBeach has been widely validated in nearshore sediment transport contexts (Ruffini et al. 2020), including those with coarse or gravel seabeds (Ruiz de Alegría-Arzaburu et al. 2010). This modeling component was used to simulate the short-term effects of both rigid and soft coastal protection structures on hydrodynamic circulation and morphology under project-specific storm surge scenarios. Using storm reanalysis data from the Copernicus Marine Environment Monitoring Service (CMEMS, https://www.mercator-ocean.eu/en/place/cmems-copernicus-marine-environment-monitoring-service/) and the high-resolution DEM of the study area, the model-chain enabled evaluation of adaptation strategies, including submerged artificial reefs, beach nourishment, and temporary dune reinforcements with sandbags (Brocchini et al., unpublished data). These simulations were instrumental in assessing the effectiveness, feasibility, and resilience of these various coastal defense measures, particularly under future climate change scenarios such as sea level rise and increased storm intensity.

Overall, the integrated geomatics-based survey addressed a methodological gap in shallow coastal mapping and provided valuable high-resolution data to support evidence-based coastal planning and risk reduction strategies in a vulnerable setting.

The relatively limited spatial extent of the survey (2 nm alongshore and 1 nm offshore) constrains direct extrapolation of site-specific results to larger coastal areas. Nevertheless, the workflow was designed as a scalable and replicable approach: although the geomorphological outcomes are locally focused, the modular framework is broadly transferable and allows individual components to be applied independently where resources for full multi-platform integration are limited. Although UAV and ASV platforms offer clear cost advantages over airborne LiDAR bathymetry or traditional crewed surveys, investment in MBES operations and specialized software may still be required depending on project objectives and budget.

As research in coastal zones increasingly moves towards holistic, process-based approaches, the seamless integration of newly purposefully acquired—such as in this study—and/or existing high-resolution topographic and bathymetric data becomes essential for accurate modeling and informed decision-making.

Acknowledgements

This study was conducted as part of a wider project finalized to the characterization and protection of the coastline of Sirolo and related cliff. It was funded by the municipality of Sirolo in agreement with the Marche Region. Authors thank Metis srl. and FlyEngineering srl. which supported the single-beam and photogrammetric survey, respectively. Special thanks to the R/V Tecnopesca II crew and to Dr. Gianna Fabi who actively contributed to the multibeam data acquisition. Her expertise and mentorship are deeply missed. This study represents partial fulfilment of the requirements for the doctoral thesis of G.S. and G.A., within the international PhD Program 'Innovative Technologies and Sustainable Use of Mediterranean Sea Fishery and Biological Resources' (FishMed-PhD; www.FishMed-PhD.org) at the University of Bologna, Italy.

Author contributions

Conceptualization, A.N.T. and P.P.; methodology, A.N.T. and P.P.; data acquisition G.S., E.S.M. and A.N.T.; formal analysis, G.S, A.N.T.; data curation, G.S., G.A., A.N.T.; writing—original draft preparation, A.N.T.; writing—review

and editing, A.N.T., G.S., G.A., M.B. E.S.M. and P.P.; supervision, P.P.; project administration, P.P.; funding acquisition, P.P. All authors have read and agreed to the published version of the manuscript.

Disclosure statement

The authors declare no conflict of interest. The funders had no role in the design of the study; in the collection, analyzes, or interpretation of data; in the writing of the manuscript, or in the decision to publish the results.

Funding

This research was funded by Service arrangement between the municipality of Sirolo, UNIVPM and CNR-IRBIM and related to the feasibility study for the protection of the beaches and related cliff. Prot. 6269 on 06.12.2022.

ORCID

Anna Nora Tassetti 0000-0001-5946-7877
Giorgio Simone 0009-0006-9575-9643
Gaspare Avanzato 0009-0005-6547-0702
Eva Savina Malinverni 0000-0001-6582-2943
Francesco Memmola 0009-0005-8003-6728
Maurizio Brocchini 0000-0003-3388-516X
Pierluigi Penna 0000-0003-1806-1576

Data availability statement

The data acquired and produced in this study are subject to a commercial agreement and are owned by a third party. As such, the data are not publicly available and cannot be shared by the authors. Access to the data may be granted by the data owner upon request and subject to the terms of the original agreement.

References

Agrafiotis P, Skarlatos D, Georgopoulos A, Karantzalos K. 2019. Shallow water bathymetry mapping from UAV imagery based on machine learning. Int Arch Photogramm Remote Sens Spat Inf Sci. XLII-2/W10:9–16. https://doi.org/10.5194/isprs-archives-XLII-2-W10-9-2019

Ahmed M, Halder B, Juneng L, Farooque A, Yaseen Z. 2025. Remote sensing-based shoreline change investigation in Klang coast and Langkawi island towards sustainable coastal management. Geomat Nat Hazards Risk. 16(1):2493226. https://doi.org/10.1080/19475705.2025.2493226

Alevizos E, Oikonomou D, Argyriou A, Alexakis D. 2022. Fusion of drone-based RGB and multi-spectral imagery for shallow water bathymetry inversion. Remote Sens. 14(5):1127. https://doi.org/10.3390/rs14051127

Baldoni A, et al. 2024. Modeling coastal inundation for adaptation to climate change at local scale: the case of Marche Region (central Italy). Front Clim. 6:1334625. https://doi.org/10.3389/fclim.2024.1334625.

Bonaldo D, et al. 2019. Integrating multidisciplinary instruments for assessing coastal vulnerability to erosion and sea level rise: lessons and challenges from the Adriatic Sea, Italy. J Coast Conserv. 23(1):19–37. https://doi.org/10.1007/s11852-018-0633-x

Booij N, Ris R, Holthuijsen L. 1999. A third-generation wave model for coastal regions: 1. Model description and validation. J Geophys Res Oceans. 104(C4):7649–7666. https://doi.org/10.1029/98JC02622

Buffi G, Manciola P, Grassi S, Barberini M, Gambi A. 2017. Survey of the Ridracoli Dam: UAV–based photogrammetry and traditional topographic techniques in the inspection of vertical structures. Geomat Nat Hazards Risk. 8(2):1562–1579. https://doi.org/10.1080/19475705.2017.1362039

Carvalho RC, Hamylton S, Woodroffe CD. 2017. Filling the 'white ribbon' in temperate Australia: A multi-approach method to map the terrestrial-marine interface2017 IEEE/OES Acoustics in Underwater Geosciences Symposium (RIO Acoustics); Rio de Janeiro, Brazil. 1–5. https://doi.org/10.1109/RIOAcoustics.2017.8349743

Colbo K, Ross T, Brown C, Weber T. 2014. A review of oceanographic applications of water column data from multibeam echosounders. Estuar Coast Shelf Sci. 145:41–56. https://doi.org/10.1016/j.ecss.2014.04.002

Cooper I, Hotchkiss R, Williams G. 2021. Extending multi-beam sonar with structure from motion data of shorelines for complete pool bathymetry of reservoirs. Remote Sens. 13(1):35. https://doi.org/10.3390/rs13010035

Danielson J, et al. 2016. Topobathymetric elevation model development using a new methodology: coastal national elevation database. J Coast Res. 76:75–89. https://doi.org/10.2112/SI76-008

Dike E, Ameme B, Efeovbokhan O. 2024. Shoreline position trends in the Niger Delta: analyzing spatial and temporal changes through Sentinel-1 SAR imagery. Geomat Nat Hazards Risk. 15(1):2346150. https://doi.org/10.1080/19475705.2024.2346150

Dong W, et al. 2023. Adaptation of coastal defence structure as a mechanism to alleviate coastal erosion in monsoon dominated coast of Peninsular Malaysia. J Environ Manage. 333:117391. https://doi.org/10.1016/j.jenvman.2023.117391

Fan C, et al. 2023. Emerging signals of coastal system changes under rapid anthropogenic disturbance in Hangzhou Bay, China. Ecol Indic. 146:109816. https://doi.org/10.1016/j.ecolind.2022.109816

Foglini F, et al. 2025. A new multi-grid bathymetric dataset of the Gulf of Naples (Italy) from complementary multi-beam echo sounders. Earth Syst Sci Data. 17(1):181–203. https://doi.org/10.5194/essd-17-181-2025

Freeman C, Bernstein D, Mitasova H. 2004. Rapid response 3D survey techniques for seamless topo/bathy modeling: 2003 Hatteras Breach. Vol. 72. Shore Beach: North Carolina.

Gesch D, Wilson R. 2001. Development of a seamless multisource topographic/bathymetric elevation model of Tampa Bay. Mar Technol Soc J. 35(4):58–64. https://doi.org/10.4031/002533201788058062

Haidvogel D, et al. 2008. Ocean forecasting in terrain-following coordinates: Formulation and skill assessment of the Regional Ocean Modeling System. J Comput Phys. 227(7):3595–3624. https://doi.org/10.1016/j.jcp.2007.06.016

Holland M, Becker A, Smith J, Everett J, Suthers I. 2021. Characterizing the three-dimensional distribution of schooling reef fish with a portable multibeam echosounder. Limnol Oceanogr Methods. 19(5):340–355. https://doi.org/10.1002/lom3.10427

Hughes Clarke J, Mayer L, Wells D. 1996. Shallow-water imaging multibeam sonars: A new tool for investigating seafloor processes in the coastal zone and on the continental shelf. Mar Geophys Res. 18(6):607–629. https://doi.org/10.1007/BF00313877

Hutchinson M. 2000. Optimising the degree of data smoothing for locally adaptive finite element bivariate smoothing splines. ANZIAM J. 42:774. https://doi.org/10.21914/anziamj.v42i0.621

Hutchinson M, Xu T, Stein J. 2011. Recent progress in the ANUDEM elevation gridding procedure. Geomorphometry. 2011:19–22.

Kenny A, et al. 2003. An overview of seabed-mapping technologies in the context of marine habitat classification☆. ICES J Mar Sci. 60(2):411–418. https://doi.org/10.1016/S1054-3139(03)00006-7

Laignel B, et al. 2023. Observation of the Coastal Areas, Estuaries and Deltas from Space. Surv Geophys. 44(5):1309–1356. https://doi.org/10.1007/s10712-022-09757-6

Legleiter C. 2012. Remote measurement of river morphology via fusion of LiDAR topography and spectrally based bathymetry. Earth Surf Process Landf. 37(5):499–518. https://doi.org/10.1002/esp.2262

Leon J, Phinn S, Hamylton S, Saunders M. 2013. Filling the 'white ribbon' – a multisource seamless digital elevation model for Lizard Island, northern Great Barrier Reef. Int J Remote Sens. 34:6337–6354. https://doi.org/10.1080/01431161.2013.800659

Lewicka O, et al. 2022. Integration data model of the bathymetric monitoring system for shallow waterbodies using UAV and USV platforms. Remote Sens. 14(16):4075. https://doi.org/10.3390/rs14164075

Li S, et al. 2022. Bathymetric LiDAR and multibeam echo-sounding data registration methodology employing a point cloud model. Appl Ocean Res. 123:103147. https://doi.org/10.1016/j.apor.2022.103147

Lubczonek J, Kazimierski W, Zaniewicz G, Lacka M. 2021. Methodology for combining data acquired by unmanned surface and aerial vehicles to create digital bathymetric models in shallow and ultra-shallow waters. Remote Sens. 14(1):105. https://doi.org/10.3390/rs14010105

Madricardo F, et al. 2019. Assessing the human footprint on the sea-floor of coastal systems: the case of the Venice Lagoon, Italy. Sci Rep. 9(1):6615. https://doi.org/10.1038/s41598-019-43027-7

Meadows M, Jones S, Reinke K. 2024. Vertical accuracy assessment of freely available global DEMs (FABDEM, Copernicus DEM, NASADEM, AW3D30 and SRTM) in flood-prone environments. Int J Digit Earth. 17(1):2308734. https://doi.org/10.1080/17538947.2024.2308734

Mills J, Buckley S, Mitchell H, Clarke P, Edwards S. 2005. A geomatics data integration technique for coastal change monitoring. Earth Surf Process Landf. 30(6):651–664. https://doi.org/10.1002/esp.1165

Minelli A, et al. 2021. Semi-automated data processing and semi-supervised machine learning for the detection and classification of water-column fish schools and gas seeps with a multibeam echosounder. Sensors. 21(9):2999. https://doi.org/10.3390/s21092999

Mudiyanselage S, Abd-Elrahman A, Wilkinson B, Lecours V. 2022. Satellite-derived bathymetry using machine learning and optimal Sentinel-2 imagery in South-West Florida coastal waters. GIScience Remote Sens. 59(1):1143–1158. https://doi.org/10.1080/15481603.2022.2100597

Pirasteh S, Li J. 2017. Landslides investigations from geoinformatics perspective: quality, challenges, and recommendations. Geomat Nat Hazards Risk. 8(2):448–465. https://doi.org/10.1080/19475705.2016.1238850

Quadros N, Collier P, Fraser C. 2008. Integration of bathymetric and topographic LiDAR: a preliminary investigation. Int Arch Photogramm Remote Sens Spat Inf Sci. 37(8):1299–1304.

Ruffini G, et al. 2020. Numerical modeling of flow and bed evolution of bichromatic wave groups on an intermediate beach using nonhydrostatic XBeach. J Waterw Port Coast Ocean Eng. 146(1):04019034. https://doi.org/10.1061/(ASCE)WW.1943-5460.0000530

Ruiz de Alegría-Arzaburu AD, Williams J, Masselink G. 2010. Application of XBeach to model storm response on a macrotidal gravel barrier. Coast Eng Proc. 32:39–39. https://doi.org/10.9753/icce.v32.sediment.39
Saeidi V, et al. 2023. Water depth estimation from Sentinel-2 imagery using advanced machine learning methods and explainable artificial intelligence. Geomat Nat Hazards Risk. 14(1):2225691. https://doi.org/10.1080/19475705.2023.2225691
Salameh E, et al. 2019. Monitoring beach topography and nearshore bathymetry using spaceborne remote sensing: a review. Remote Sens. 11(19):2212. https://doi.org/10.3390/rs11192212
Shih H, et al. 2024. Monitoring and risk assessment of Taoyuan ponds using an unmanned surface vehicle with multibeam echo sounder, ground-penetrating radar, and electrical resistivity tomography. Geomat Nat Hazards Risk. 15(1):2323598. https://doi.org/10.1080/19475705.2024.2323598
Smit P, et al. 2010. XBeach: Non-hydrostatic model. Tech Rep Delft Univ Technol Deltares.
Somoza L, et al. 2021. High-resolution multibeam bathymetry of the northern Mid-Atlantic Ridge at 45–46° N: the Moytirra hydrothermal field. J Maps. 17(2):184–196. https://doi.org/10.1080/17445647.2021.1898485
Stanghellini G, et al. 2022. Repeated (4D) marine geophysical surveys as a tool for studying the coastal environment and ground-truthing remote-sensing observations and modeling. Remote Sens. 14(22):5901. https://doi.org/10.3390/rs14225901
Stanghellini G, Del Bianco F, Gasperini L. 2020. OpenSWAP, an open architecture, low cost class of autonomous surface vehicles for geophysical surveys in the Shallow water environment. Remote Sens. 12(16):2575. https://doi.org/10.3390/rs12162575
Starek M, Giessel J. 2017. Fusion of uas-based structure-from-motion and optical inversion for seamless topo-bathymetric mapping. IEEE: Fort Worth, TX. p 2999–3002. https://doi.org/10.1109/IGARSS.2017.8127629
Szostak R, Pietroń M, Wachniew P, Zimnoch M, Ćwiąkała P. 2024. Estimation of small-stream water surface elevation using UAV photogrammetry and deep learning. Remote Sens. 16(8):1458. https://doi.org/10.3390/rs16081458
Tassetti A, Malaspina S, Fabi G. 2015. Using a multibeam echosounder to monitor an artificial reef. Int Arch Photogramm Remote Sens Spat Inf Sci. XL-5/W5:207–213. https://doi.org/10.5194/isprsarchives-XL-5-W5-207-2015
Troiani F, et al. 2020. Integrated field surveying and land surface quantitative analysis to assess landslide proneness in the conero promontory rocky coast (Italy). Appl Sci. 10(14):4793. https://doi.org/10.3390/app10144793
Uunk L, Wijnberg K, Morelissen R. 2010. Automated mapping of the intertidal beach bathymetry from video images. Coast Eng. 57(4):461–469. https://doi.org/10.1016/j.coastaleng.2009.12.002
Wahba G. 1990. Spline models for observational data. Philadelphia: Society for Industrial and Applied Mathematics.
Ward N, et al. 2020. Representing the function and sensitivity of coastal interfaces in Earth system models. Nat Commun. 11(1):2458. https://doi.org/10.1038/s41467-020-16236-2
Warner J, Armstrong B, He R, Zambon J. 2010. Development of a coupled ocean–atmosphere–wave–sediment transport (COAWST) modeling system. Ocean Model. 35(3):230–244. https://doi.org/10.1016/j.ocemod.2010.07.010
Westhead K, Smith K, Campbell E, Colenutt A, McVey S. 2014. Pushing the boundaries: Integration of multi-source digital elevation model data for seamless geological mapping of the UK's coastal zone. Earth Environ Sci Trans R Soc Edinb. 105(4):263–271. https://doi.org/10.1017/S1755691015000134
Włodarczyk-Sielicka M, Bodus-Olkowska I, Łącka M. 2022. The process of modelling the elevation surface of a coastal area using the fusion of spatial data from different sensors. Oceanologia. 64(1):22–34. https://doi.org/10.1016/j.oceano.2021.08.002
Xu N, Wang L, Ma Y, Ma X, Wang X. 2025. Constructing intertidal topography for sandy beaches by combining Sentinel-2 imagery and water level data. Geo-Spat Inf Sci. 1–15. https://doi.org/10.1080/10095020.2024.2449453